SIViP (2014) 8:423–432
DOI 10.1007/s11760-012-0304-6

ORIGINAL PAPER

Incremental variations of image moments for nonlinear image registration

Wei Liu · Eraldo Ribeiro

Received: 9 April 2011 / Revised: 9 March 2012 / Accepted: 10 March 2012 / Published online: 28 March 2012

Abstract In this paper, we use image moments to solve the problem of estimating deformation fields given a pair of images as input. We use a single family of polynomials to parameterize the deformation field and to define image moments. In this way, variations in image moments can be represented by a set of linear equations. We solve these equations iteratively for the deformation parameters between two shapes. Our approach improves existing moment-based registration methods in both robustness to noise and convergence rate. In addition, our method does not rely on solving the correspondence problem. We have extensively tested our new method on both synthetically deformed MPEG-7 shapes and real-world biomedical images.

Keywords Image moments · Shape deformation · Shape registration · Polynomial deformation

1 Introduction

Registration is a fundamental problem in computer vision, having the main goal of aligning images that have undergone geometric transformations. Applications of registration include shape retrieval, object recognition [1], and medical image analysis [2]. In this paper, we propose a novel image-registration method based on image moments [3] and incremental optimization. The method estimates image deformation without the need for feature correspondence.

Our main contribution is a robust registration method that uses image moments and fixed-point iterative optimization. The method is based on a novel observation: By using polynomials to model the deformation field between two images, moments calculated on these images are related through a system of linear equations of the deformation parameters. We solve this linear system for the deformation parameters using an iterative fixed-point optimization method that converges in a few steps without a costly gradient-based search, while being more robust than other moment-based registration methods [1,4].

Our method is related to recent works by Flusser et al. [4], and Domokos and Kato [1]. In fact, our cost function can be seen as a special case of the "implicit moment invariants" [4]. However, we adopt a different optimization approach by iteratively solving for the deformation parameters (i.e., incremental registration), which simplifies the evaluation of the gradient function. Our experiments show that our method is more robust than the one by Domokos and Kato [1]. Although image moments are used in both our work and the one in [4], the two approaches have distinct aims. In [4], the focus is on retaining image-invariance properties under deformations. In contrast, ours measures incremental deformations from moments. Also, our registration method does not need prior information about the object's shape. These merits are shared with Flusser's method [4].

This paper extends our previous work [5]. Here, we adopt a weak-form formulation of the registration problem using integral transforms and derive their incremental variation for polynomial image deformation. We also design and compare two iterative solutions for our registration method: a fixed-point iteration and a gradient-descent search. Finally, we performed extensive experiments on a variety of synthetic and real-world images.

The remainder of this paper is organized as follows. Section 2 reviews the related work. Section 3 introduces the integral-transform formulation of the registration problem.

W. Liu · E. Ribeiro (✉)
Computer Vision Laboratory, Department of Computer Sciences, Florida Institute of Technology, Melbourne, FL, USA
e-mail: eribeiro@cs.fit.edu

In Sect. 4, we analyze the variation of integral transforms under nonrigid image deformation, parameterized as a linear combination of basis functions. Here, we also describe the main steps of our registration algorithm. Finally, in Sect. 5, we test our registration method on synthetic and real-world images of shapes and gray-scale objects. We also compare our method with a classic intensity-based approach and with a recently proposed moment-based method [1]. The results demonstrate the method's robustness to both noise and occlusion as well as having a good convergence rate.

2 Related work

Image-registration methods usually differ in three main aspects [6]: the similarity measure, the deformation model, and the optimization process. Similarity measures quantify the registration quality by comparing the target image with a deformed source image. Most similarity measures are based on feature matching or pixelwise correspondence. A good review of similarity measures for image registration is found in [6]. The deformation models provide compact and often parametric representations of image deformations. Optimization processes search for optimal deformation parameters that maximize the similarity measure.

Image similarity can also be measured indirectly in a transform domain. For example, early work by De Castro and Morandi [7] uses the Fourier transform's shift and rotation properties for registering images. The method was later extended by Chen et al. [8] and also by Lehmann [9] to also address scaling transformations. Registration methods for nonrigid transformations such as affine [10] and polynomial deformations [5,11] have also been proposed.

Some registration methods have also used other types of integral transforms such as texture moments [10], log-polar transforms [12], and wavelet transforms [11,13]. Table 1 lists some registration methods that are based on integral transforms. Note that some methods use integral transforms as *local* feature descriptors. For example, Shen et al. [14] calculated image moments in the neighborhood of a voxel as feature descriptors for nonrigid registration. These methods rely on solving the correspondence problem and are not discussed further in this paper.

Recently, Domokos and Kato [1] proposed a moment-based registration method by solving polynomial equations derived from shape moments. Our method is different from theirs in many aspects. First, we extend the affine model to a more general polynomial model. Secondly, our method iteratively warps the source image into the target image. Domokos and Kato's method [1] registers two shapes with a single step by solving a polynomial system. Despite its computational efficiency, solving a polynomial system directly is sensitive to noise and occlusion. These complicating factors are less of an issue to our method as shown by our experiments. Another key difference between our method and the one in [1] is that ours is not restricted to binary images, working for both binary and gray-scale images. Finally, we define both the deformation field and moments using the same family of basis polynomials, leading to a simplified computation procedure. Polynomials have been shown to be effective in modeling nonrigid motion fields [18]. To the best of our knowledge, our work is the first to study the interplay between polynomial models and image moments.

The closest work to ours is that of Flusser et al. [4], which matches patterns using image moments under polynomial deformations. In contrast, we analyze the interaction between

Table 1 Literature summary

Year	Author	Integral transform	Deformation
1987	De Castro and Morandi [7]	Fourier	Translation, rotation
1994	Chen et al. [8]	Fourier-Mellin	Translation, rotation, scaling
1995	Sato and Cipolla [10]	Texture moments	Affine
1998	Lehmann [9]	Fourier-Mellin	Translation, rotation, scaling
2002	Lucchese et al. [15]	Fourier	Affine
2002	Moigne et al. [11]	Wavelets	Polynomial
2005	Bentoutou et al. [13]	Wavelets	Affine
2005	Zokai and Wolberg [12]	Log-polar	Projective
2008	Ito et al. [16]	Wavelets	Affine
2010	Domokos and Kato [1]	Image moments	Affine
2010	Flusser et al. [4]	Image moments	Polynomial
2010	Our work [5]	Image moments	Polynomial
2011	Crespo and Aguiar [17]	Complex moments	Affine

image moments and incremental deformations to obtain a gradient function in an analytic form. Also, we propose a fixed-point registration algorithm, which is shown to be more robust to noise and achieve faster convergence than a gradient-descent method equivalent to the one in [4].

Finally, a recent work by Crespo and Aguiar [17] revisited the complex image moments for 2-D shape representation by extending the classic moment invariants [19]. Please refer to [19] for a review of image moments and their applications to shape recognition and registration.

3 An integral-transform formulation of the image-registration problem

Our goal is to find the geometric transformation $\mathbf{T}$ between a template image f and a target image f', under the assumption that f' is a deformed version of f. Following the existing literature [6], we represent $\mathbf{T}$ using a deformation field $\mathbf{u}$ and write the transformed image coordinates as $\mathbf{x}' = \mathbf{T}(\mathbf{x}) = \mathbf{x} + \mathbf{u}(\mathbf{x})$, where $\mathbf{x}$ is the coordinate vector. Most image-registration methods assume that pixel intensity remains constant after deformation [4], that is,

$$f(\mathbf{x}) = f'(\mathbf{x}'), \quad \mathbf{x}' = \mathbf{x} + \mathbf{u}(\mathbf{x}), \quad \mathbf{x} \in \Omega, \tag{1}$$

where Ω is the image domain. The constraint in (1) is often enforced by minimizing the squared-sum of registration residue (SSD) given by:

$$E_{\text{ssd}} = \int_{\Omega} \left(f(\mathbf{x}) - f'(\mathbf{x}')\right)^2 \mathrm{d}\mathbf{x}. \tag{2}$$

In this paper, we will call Eq. 1 the *strong form* of the similarity function, as it relies on the intensities of corresponding pixels. This intensity-constancy assumption may be violated because of noise and changes in illumination. To relax this assumption, we propose a modified version of (1), by multiplying both sides of that equation by kernel (test) functions ϕ_l, and integrating as follows:

$$\int_{\Omega} f(\mathbf{x})\phi_l(\mathbf{x})\mathrm{d}\mathbf{x} = \int_{\Omega} f'(\mathbf{x}')\phi_l(\mathbf{x}')\mathrm{d}\mathbf{x}', \quad l = 1, \ldots, L. \tag{3}$$

From (3), a new similarity measure can be written as:

$$E_{\text{weak}} = \sum_{l=1}^{L} \left(\langle f, \phi_l\rangle - \langle f', \phi_l\rangle\right)^2, \tag{4}$$

where

$$\langle f, \phi_l\rangle = \int_{\Omega} f(\mathbf{x})\phi_l(\mathbf{x})\mathrm{d}\mathbf{x} \tag{5}$$

and

$$\langle f', \phi_l\rangle = \int_{\Omega} f'(\mathbf{x}')\phi_l(\mathbf{x}')\mathrm{d}\mathbf{x}' \tag{6}$$

are the integral transforms of $f(\mathbf{x})$ and $f'(\mathbf{x}')$, respectively, using kernel functions ϕ_l [20]. Equation 3 conceptually similar to the implicit moment invariants was proposed by Flusser et al. [4]. Our formulation is an alternative interpretation that enforces image similarity for registration. More specifically, Eq. 3 is a *weaker* condition than that in Eq. 1, as Eq. 3 is only necessary but not sufficient condition for Eqs. 1. For example, consider two binary images of an object and a single test function $\phi_1 = 1$. Then, $\langle f, \phi_1\rangle$ and $\langle f', \phi_1\rangle$ are the areas of the object in the template and target images, respectively. In this example, satisfying (3) implies a pixelwise alignment based on equal areas. However, objects of equal area are not necessarily aligned. As a result, we will call Eq. 3 the *weak-form* registration constraint and Eq. 4 the *weak-form* SSD.

The weak-form constraint becomes the strong form for a sufficient number of test functions.[1] In this paper, we formulate a solution to the image-registration problem using the weak-form constraint using monomials $\phi_l(x, y) = x^s y^t$ with $s, t \geq 0$ as test functions. For this choice of test function, the integral transforms in (3) correspond to image moments [3].

Robustness to noise and occlusion, and computation efficiency are key motivations in using moments (and integral transforms) for image registration. Moments have been shown to be robust to noise when used as affine-invariant descriptors in shape retrieval [21]. We observe similar robustness when using moments to analyze nonrigid deformations. Efficient algorithms can be proposed for the more general polynomial deformation models because image deformation and image moments can be related by a system of linear equations (Sect. 4.4). In addition, our weak-form constraint measures image deformation in the compressed transform domain with no reliance on pixel correspondence. By storing only the moments of target shapes, template images can be quickly compared with many target images with potential applications to group and data-driven registration [22]. Finally, filtering capabilities of some integral transforms (e.g., wavelets, Fourier transform) help reduce the effects of noise and illumination variations [11].

4 Relating image moments and the polynomial deformation model

4.1 Polynomial deformation model

To recover the deformation field between images, the weak-form SSD in (4) can be minimized using existing numerical schemes (e.g., gradient-descend). For efficiency, we reduce the dimensionality of the solution space by representing the

[1] In the extreme case, for each pixel (x_i, y_i), one can define a test function $\phi_i(x, y) = \delta_{x_i, y_i}(x, y)$, that is, the Dirac sampling function, and then the weak form becomes the strong form.

deformation field $\mathbf{u}(\mathbf{x})$ as a linear combination of basis functions $\gamma_i(\mathbf{x})$, with $i = 1, \ldots, M$ as follows:

$$\mathbf{u} = \sum_i \mathbf{a}_i \gamma_i, \tag{7}$$

where $\mathbf{a}_i$ is the vector of coefficients. The matrix form of Eq. 7 is $\mathbf{u} = \mathbf{A}^\mathsf{T}\Gamma$, where $\mathbf{A}$ is the coefficient matrix, that is, $\mathbf{A} = (\mathbf{a}_1, \mathbf{a}_2, \ldots, \mathbf{a}_M)^\mathsf{T}$, and $\Gamma = (\gamma_1, \ldots, \gamma_M)^\mathsf{T}$ is a vector of basis functions. With this linear representation, the solution space is reduced to a lower-dimensional parametric space. In this paper, we investigate the use of a deformation model in which the deformation basis functions γ_i are bivariate monomials (i.e., of the same type as our test functions). This model includes the affine deformation as a special case (i.e., $\Gamma = (1, x, y)^\mathsf{T}$). Next, we formulate the variation of integral transforms for polynomial deformations.

4.2 Incremental variations of integral transforms

We commence by describing the effect of nonrigid deformation on integral transforms, which is the common foundation for many moment-based shape analysis and registration methods [4,1]. We will focus on the integral transform of the target image as given by the right-hand side of Eq. 3 (i.e., $\langle f', \phi_l \rangle$). By substituting the transformation $\mathbf{x}' = \mathbf{T}(\mathbf{x})$ into the integral transform $\langle f', \phi_l \rangle$, and making the appropriate change of variables, the effect of the transformation can be written as [4,1]:

$$\int_\Omega f'(\mathbf{x}')\phi_l(\mathbf{x}')d\mathbf{x}' = \int_\Omega f(\mathbf{x}) \underbrace{|\mathbf{J_T}|\, \phi_l(\mathbf{T}(\mathbf{x}))}_{\text{deformed kernel}} d\mathbf{x}. \tag{8}$$

Here, the $\mathbf{J_T} = \frac{\partial \mathbf{T}}{\partial \mathbf{x}}$ is the Jacobian of the transformation and $|\mathbf{J_T}|$ is its determinant. Under the change of coordinates, the role of $|\mathbf{J_T}|$ in (8) is to measure the infinitesimal area-scaling effect of $\mathbf{T}$ [23]. As a result, the target image's integral transform is equivalent to the integral transform of the original template image $f(\mathbf{x})$ with the deformed test function $|\mathbf{J_T}|\, \phi_l(\mathbf{T}(\mathbf{x}))$. Equation 8 is the common basis shared by [4] and our work. However, Flusser et al. [4] used Eq. 8 as an implicit form of *invariants*, while our focus is on analyzing its linear approximation for iterative registration.

From Eq. 8, the scaling factor $|\mathbf{J_T}|$ can be computed from the variation of shape areas when transformation $\mathbf{T}$ is affine and source and target shapes are not occluded. In addition, if the kernel function ϕ_i is polynomial, then (8) can be expanded into a polynomial system, leading to the direct approach described in [1]. However, this approach is limited to affine models and is unable to handle occlusions.

In our method, we approximate Eq. 8 and optimize E_{weak} in (4) using an iterative approach, in contrast to the direct approach in [1]. The derivation we propose next also differs from the "implicit moment invariants" in [4].

4.3 Incremental approximation of moment variations

We begin by approximating the Jacobian determinant in (8) as follows:

$$|\mathbf{J_T}| \approx 1 + \text{div}(\mathbf{u}), \tag{9}$$

where $\text{div}(\mathbf{u})$ is the divergence of $\mathbf{u}$ given by:

$$\text{div}(\mathbf{u}) = \sum_j \frac{\partial u^{(j)}}{\partial x^{(j)}} = \sum_j \sum_i a_i^{(j)} \frac{\partial \gamma_i}{\partial x^{(j)}}. \tag{10}$$

The above approximation is based on the assumptions that the magnitude of the deformation field $\mathbf{u}$ is small and that, because $\mathbf{u}$ is represented by low-order polynomials, its derivatives $\frac{\partial \mathbf{u}}{\partial \mathbf{x}}$ are both bounded and small [23]. To avoid confusion with indices of polynomials, we use lowercase letters and letters with parenthetical superscripts to indicate the components of a vector. For example, we may denote a 2-D vector as $\mathbf{x} = (x, y)^\mathsf{T}$ or $\mathbf{x} = \left(x^{(1)}, x^{(2)}\right)^\mathsf{T}$. As in (9), the deformed kernel function $\phi_l(\mathbf{T}(\mathbf{x}))$ is linearized as:

$$\begin{aligned}\phi_l(\mathbf{x} + \mathbf{u}) &= \phi_l(\mathbf{x}) + \mathbf{u}^\mathsf{T} \frac{\partial \phi_l}{\partial \mathbf{x}} \\ &= \phi_l(\mathbf{x}) + \sum_j \sum_i a_i^{(j)} \frac{\partial \phi_l}{\partial x^{(j)}} \gamma_i. \end{aligned} \tag{11}$$

We can now obtain an expression for the variation of integral transforms with respect to incremental deformations. To do this, we substitute the linearized Jacobian determinant in (9) and the linearized deformed kernel function in (11) into (8) and ignore higher-order terms, i.e.,:

$$\begin{aligned}\langle f', \phi_l \rangle &\approx \int_\Omega \left(\phi_l(\mathbf{x}) + \frac{\partial \phi_l}{\partial \mathbf{x}}\mathbf{u}\right) f(\mathbf{x})\,(1 + \text{div}(\mathbf{u}))\, d\mathbf{x} \\ &\approx \underbrace{\int_\Omega \phi_l(\mathbf{x}) f(\mathbf{x}) d\mathbf{x}}_{\text{original moment}} + \underbrace{\int_\Omega \frac{\partial \phi_l}{\partial \mathbf{x}} \mathbf{u} f(\mathbf{x}) d\mathbf{x}}_{\text{shape variation}} \\ &\quad + \underbrace{\int_\Omega \phi_l(\mathbf{x}) f(\mathbf{x}) \text{div}(\mathbf{u}) d\mathbf{x}}_{\text{area variation}} \\ &= \langle f, \phi_l \rangle + \sum_j \sum_i a_i^{(j)} \int_\Omega \frac{\partial \phi_l}{\partial x^{(j)}} \gamma_i f(\mathbf{x}) d\mathbf{x} \\ &\quad + \sum_j \sum_i a_i^{(j)} \int_\Omega \phi_l(\mathbf{x}) \frac{\partial \gamma_i}{\partial x^{(j)}} f(\mathbf{x}) d\mathbf{x} \\ &= \langle f, \phi_l \rangle + \sum_j \sum_i a_i^{(j)} \\ &\quad \times \left(\langle f, \frac{\partial \phi_l}{\partial x^{(j)}} \gamma_i \rangle + \langle f, \phi_l \frac{\partial \gamma_i}{\partial x^{(j)}} \rangle\right). \end{aligned} \tag{12}$$

Next, we further simplify Eq. 12 by using the same family of monomials to represent both the test functions ϕ_l and

the deformation bases γ_i. This simplification allows us to implement an efficient registration algorithm.

4.4 Efficient gradient computation using polynomials

The incremental variation of the integral transform w.r.t. deformation parameters, i.e., the gradient of $\langle f, \phi_l \rangle$, is given by:

$$\frac{\partial \langle f, \phi_l \rangle}{\partial a_i^{(j)}} = \left\langle f, \frac{\partial \phi_l}{\partial x^{(j)}} \gamma_i \right\rangle + \left\langle f, \phi_l \frac{\partial \gamma_i}{\partial x^{(j)}} \right\rangle = \left\langle f, \frac{\partial \phi_l \gamma_i}{\partial x^{(j)}} \right\rangle. \quad (13)$$

If we chose kernel functions ϕ_l and polynomial basis functions γ_i to be monomials of the same type, $\phi_l = x^p y^q$ and $\gamma_i = x^s y^t$ ($s, t \in \mathbb{Z}$, $s, t \geq 0$ and $p, q \in \mathbb{Z}$, $p, q \geq 0$), then the integral transforms become the classical image moments, i.e.,:

$$\begin{aligned} \langle f, \phi_l \rangle &= \langle f, x^p y^q \rangle \\ &= M_{p,q} = \iint_{\Omega} x^p y^q f(x, y) \, \mathrm{d}x \, \mathrm{d}y, \end{aligned} \quad (14)$$

and the components of the deformation field in (7) become:

$$\begin{aligned} u(x, y) &= \sum_{s=0}^{N} \sum_{t=0}^{N} a_{s,t} \, x^s y^t \quad \text{and} \quad v(x, y) \\ &= \sum_{s=0}^{N} \sum_{t=0}^{N} b_{s,t} \, x^s y^t, \end{aligned} \quad (15)$$

Because monomials are closed under differentiation and multiplication, the terms $\frac{\partial \phi_l \gamma_i}{\partial x^{(j)}}$ in Eq. 13 are also monomials. Substituting $\phi_l = x^p y^q$ and $\gamma_i = x^s y^t$ into (13), we have:

$$\begin{aligned} \frac{\partial M_{p,q}}{\partial a_{s,t}} &= \frac{\partial \langle f, \phi_l \rangle}{\partial a_{s,t}} \\ &= \langle f, \frac{\partial x^{p+s} y^{q+t}}{\partial x} \rangle = (p + s) M_{p+s-1,q+t}, \end{aligned} \quad (16)$$

and

$$\begin{aligned} \frac{\partial M_{p,q}}{\partial b_{s,t}} &= \frac{\partial \langle f, \phi_l \rangle}{\partial a_{s,t}} \\ &= \left\langle f, \frac{\partial x^{p+s} y^{q+t}}{\partial y} \right\rangle = (q + t) M_{p+s,q+t-1}. \end{aligned} \quad (17)$$

Finally, by substituting (14), (16), and (17) into the linearized variation in Eq. 12, we show that the moments of the deformed image can be approximated as a linear combination of the original image moments, i.e.,:

Algorithm 1: Registration using fixed-point iteration.

Input: Template I_s, target image I_t, deformation basis γ_i, and test functions ϕ_i.
Output: Deformation parameters $\mathbf{a}$.
Initialize $\mathbf{a}^0 \leftarrow 0$;
Initialize currently deformed template image $I_s^0 = I_s$;
Calculate image moments of the target image $\langle I_t, \phi_i \rangle$;
while *Not converge* **do**
  Calculate image moments of the deformed template image $\langle I_s^k, \phi_i \rangle$;
  Solve the linear system given by stacking Eq. 18;
  Obtain current incremental deformation parameters $\Delta\mathbf{a}$;
  Update $\mathbf{a}^{k+1} = \mathbf{a}^k + \Delta\mathbf{a}$ and warp $I_s^{k+1} \leftarrow I_s^0 \left(\mathbf{x} + \mathbf{u}(\mathbf{a}^{k+1})\right)$;
end

$$\begin{aligned} M'_{p,q} \approx M_{p,q} &+ \sum_{s=0}^{N} \sum_{t=0}^{N} \left(a_{s,t} (p + s) M_{s+p-1,t+q} \right) \\ &+ \sum_{s=0}^{N} \sum_{t=0}^{N} \left(b_{s,t} (q + t) M_{s+p,t+q-1} \right). \end{aligned} \quad (18)$$

In Eq. 18, we obtained an analytic form of the incremental changes in image moments due to polynomial image deformation. This is our main contribution in comparison with previous works [4]. The relationship in (18) coincides with our approximation-theory derivation in [5]. Next, we use this analytic form to solve the registration problem.

4.5 Image registration using the weak form

We can now optimize the quantity E_{weak} in (4) to obtain an estimate of the deformation field $\mathbf{u}$ as follows:

$$\mathbf{u} = \arg\min_{\mathbf{u}} E_{weak} = \arg\min_{\mathbf{u}} \sum_{l=1}^{L} \left(\langle f, \phi_l \rangle - \langle f', \phi_l \rangle \right)^2. \quad (19)$$

A way to solve this optimization is to note that Eq. 18 defines a linear constraint for each test function and that those can be stacked together to form an overdetermined linear system of equations. To solve this system of equations, we developed a fixed-point iteration algorithm (Algorithm 1). The algorithm avoids numerical deterioration from repetitive image interpolations by obtaining a deformed template image from the original input for each iteration, instead of using the image from the previous iteration. Alternatively, we can minimize E_{weak} using gradient descent in which the gradients are given by Eq. 13. In this case, it becomes a variation of Flusser's method [4]. For completeness, we summarize the process in Algorithm 2.

5 Experiments

Our experiments are divided into two main parts. We begin by assessing the effects of the input parameters of our method.

Algorithm 2: Registration using gradient descent.

Input: Template I_s, target image I_t, deformation basis γ_i, and kernel functions ϕ_i.
Output: Deformation parameters a.
Initialize $\mathbf{a}^0 \leftarrow 0$;
Initialize $I_s^0 \leftarrow I_s$;
Calculate moments of the target image $\langle I_t, \phi_i \rangle$;
while *Not converge* **do**
  Calculate moments of the source image $\langle I_s^k, \phi_i \rangle$;
  Calculate Jacobian matrix J from $\langle I_s, \phi_i \rangle$ and $\langle I_t^k, \phi_i \rangle$ (Eq. 18);
  Update $\mathbf{a}^k$ by gradient descent using J. Warp $I_s^{k+1} \leftarrow I_s^k(\mathbf{x} + \mathbf{u}(\mathbf{a}^k))$
end

We then provide a comparison between our method and two related image-registration approaches.

We used binary images from a shape dataset as well as gray-scale medical images. For the shape dataset, we compared our method with the classic Lucas–Kanade method [24] and the recently proposed moment-based method by Domokos and Kato [1]. Our goal was twofold. First, we evaluated our algorithm on the robustness, accuracy, and computational cost. Our second goal was to show that our iterative registration achieves increased robustness and accuracy, by comparing our method with the direct method in [1]. An implementation of Flusser's method [4] was not available, but we believe that the gradient-descent method in Algorithm 2 is a comparable approximation. Finally, we applied our method on noisy medical images. Source-code of our implementation and some of the test data are available online.[2]

5.1 Analysis of the parameters of our method

The two input parameters are the number of basis functions M in the deformation model (Eq. 7), and the number of test functions L in the weak-form SSD (Eq. 4).

However, higher-order moments are numerically more sensitive than lower-order ones as we will show later. For a fixed L, we chose low-order test functions before selecting higher-order ones. To select L, we applied our method to register randomly deformed MPEG-7 shapes and compared the registration results for different values of L. Specifically, we selected 10 shapes from MPEG-7, each of which was deformed 20 times. Then, we added 5 percent of salt-and-pepper noise to both the original and the deformed shapes. Finally, we registered the original shapes to the deformed shapes and obtained two measures: the likelihood of successful convergence and the average angular error (AAE) of the converged cases. Figure 1 shows the convergence rate and AAE as functions of L. In general, as L increased, the convergence rate increased while AAE decreased.

Moments of different orders seem to have an uneven effect on the registration robustness and accuracy. Specifically, when $L = 7$, the convergence rate decreased significantly (Fig. 1a). We believe that this happens because the test functions for $L = 7$ are $\{1, x, y, x^2, xy, y^2, x^3\}$, which include uneven contributions from moments of different orders. In this case, x^3 is the only third-order term and is biased toward shape variations in the x-axis direction. For $L > 7$, other moments with balancing contributions are included. The effect of uneven contribution from moments was also evident in the AAE of the converged cases (Fig. 1b). For the results shown in Fig. 1, we chose L resulting in the highest convergence rate, while producing registrations with fairly low AAE. For the affine-deformation experiments, the deformation basis was $\Gamma = (1, x, y)^\mathsf{T}$ (i.e., $M = 3$), and we chose $L = 12$. For the second-order polynomials with $\Gamma = \left(1, x, y, x^2, xy, y^2\right)^\mathsf{T}$, we performed similar experiments and chose $L = 20$.

5.2 Comparison with existing methods

We compared our method with Domokos–Kato's method [1] which is based on moments. The tests focused on robustness and accuracy, using the MPEG-7 shape dataset [25]. First, we deformed the images using randomly generated affine transformations $\mathbf{a} = \mathbf{id} + \Delta\mathbf{a}^\mathsf{T}$, where $\mathbf{id}$ is the identity transform, with increasing perturbation magnitude $\|\Delta\mathbf{a}^\mathsf{T}\| = \max(|\Delta a_i|, i = 1, \ldots, M)$. Salt-and-pepper noise was added to all images. The shapes were then registered using both ours and Domokos–Kato's method [1].[3] Figure 2 shows the convergence rate and AAE as functions of the deformation magnitude $\|\Delta\mathbf{a}^\mathsf{T}\|$ and the percentage of image noise.

Our method consistently outperformed Domokos and Kato's method. Figure 3 shows two examples for which Domokos and Kato's method failed while our method produced good alignment. Their method seems to be sensitive to small amounts of occlusion when noise level is high.

We further compared our method with an intensity-based method to demonstrate the benefits of moment-based registration. Here, we implemented the classic Lucas–Kanade method [24] using the same polynomial deformation model used in our method. The only difference between the two implementations is that our method used the integral-transform constraint, while Lucas–Kanade's used the intensity-based constraint. Figure 4 shows registration sequences obtained using the two implementations of our method (i.e., fixed-point and gradient descent) and Lucas–Kanade's. Both

[2] http://www.cs.fit.edu/~eribeiro/icpr2010moments/

[3] Source-code available from http://www.inf.u-szeged.hu/~kato/

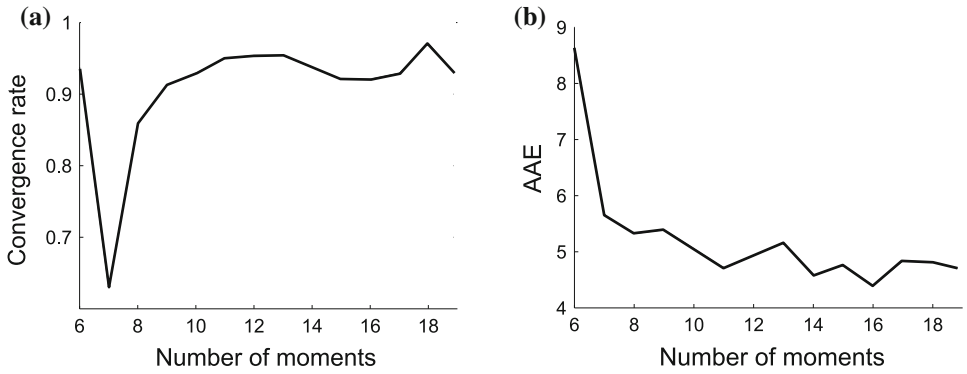

Fig. 1 Convergence rate (**a**) and average angular error (**b**) for increasing numbers of moments L. Robustness and accuracy of our method increases with L. Moments of different orders have an uneven effect

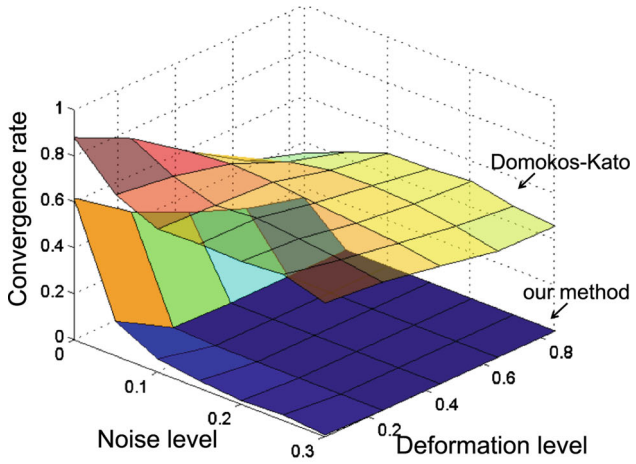

(a) Convergence rate

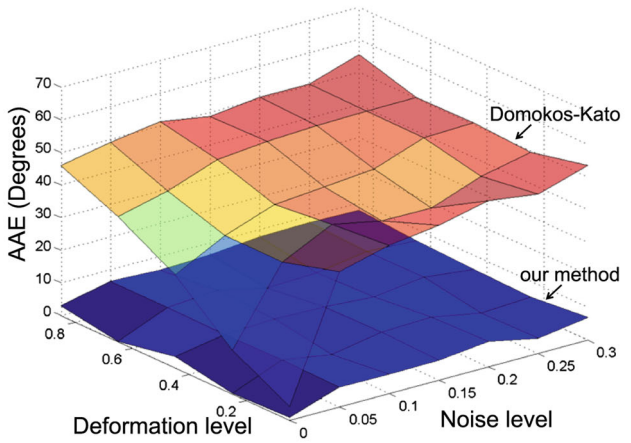

(b) Average angular error (AAE)

Fig. 2 Comparison of our method with Domokos–Kato's method. **a** Our method (*top*) achieves consistently higher convergence rate than Domokos–Kato's method (*bottom*). **b** AAE of the final results: Our method (*bottom*) outperformed Domokos–Kato's method (*top*)

implementations of our method converged in less iterations. Although each iteration of our method involves computation of image moments, the reduction in iteration steps is a positive point for future optimization.

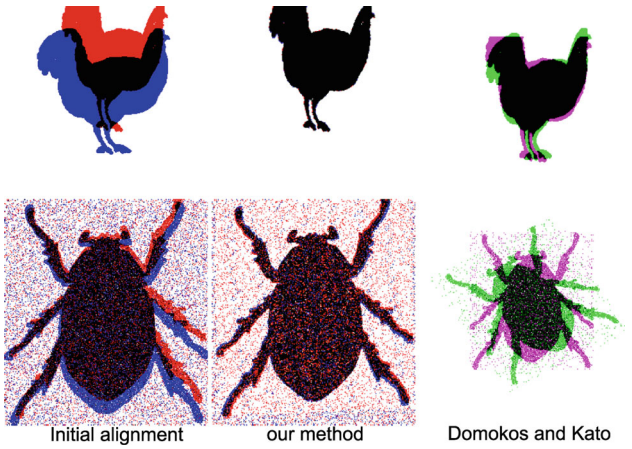

Fig. 3 Comparison of our method with Domokos–Kato's. Registration of occluded shapes. Domokos–Kato's method was affected by occlusions, but our method could still register the shapes

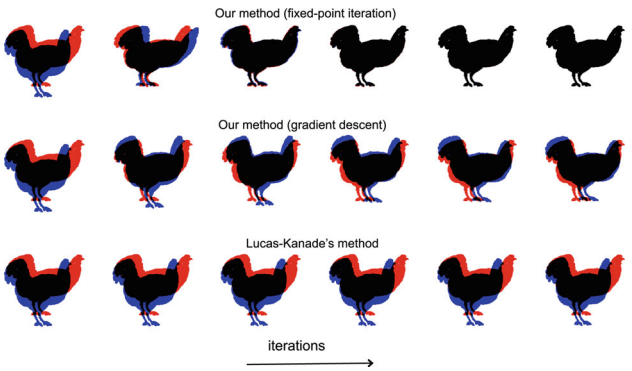

Fig. 4 Registration sequences. The source image (*red*) is iteratively warped to the target image (*blue*), shown as a sequence from left to right. Row 1: our method using fixed-point iteration. Row 2: our method using gradient descent. Row 3: Lucas–Kanade's method (color figure online)

For a quantitative comparison, we calculated both the average angular error (AAE) and the average end-point error (AEP) of the estimated deformation field at each iteration (Fig. 5a, b, respectively). The fixed-point algorithm (red curve) converged in less than five iterations, while the gradient descent (pink curve) fluctuated. Even with the

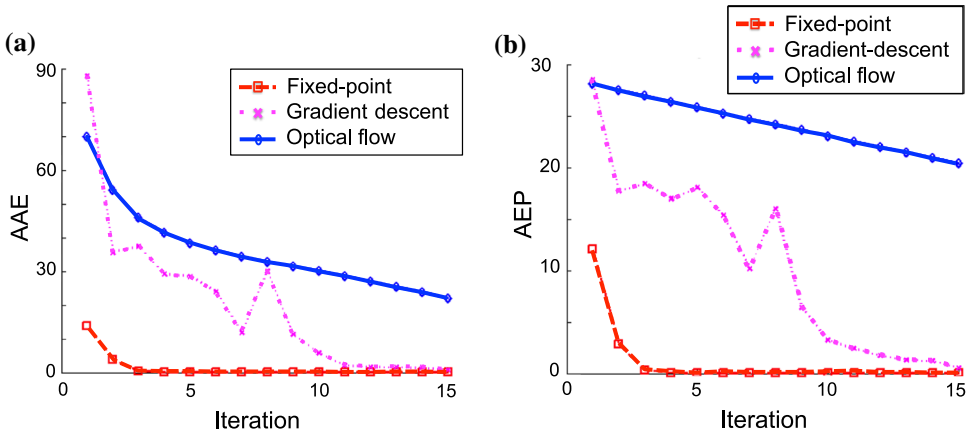

Fig. 5 Convergence plots. **a** Average angular error. **b** Average end-point error. Optical-flow method converges much slower for noisy images, while our method is less affected

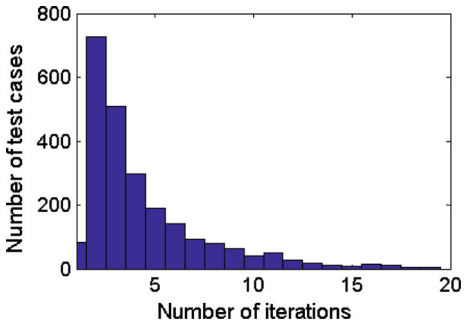

Fig. 6 Our method's number of iterations to convergence (2,000 cases)

fluctuations, our gradient-descent algorithm still converged in less steps than Lucas–Kanade's optical-flow method (blue curve). Registration error was reduced at a constant rate for the optical-flow method, while our fixed-point iteration reduced the registration error at an exponential rate. The fixed-point method was more robust and converged in less steps than the gradient-descent method. Given the equivalence between this gradient-descent method and the method by Flusser et al. [4], these results clearly indicate that our iterative fixed-point method is an improvement over [4].

To further illustrate our method's convergence behavior, Fig. 6 shows the histogram of iteration numbers for 2,000 test cases. These test cases were also used to produce the AAE and APE plots in Fig. 2. Most tests converged within five iterations. For the next experiments, we will report results produced using the fixed-point method only.

A benefit of the moment-based methods is their robustness to noise and occlusion. Figure 7 shows registration results on occluded and noisy shapes. Here, we added salt-and-pepper noise with occurrence probability of 0.3. Figure 7 shows convergence plots of our method compared to Lucas–Kanade's method. Lucas–Kanade's converged slowly for noisy images, while our method converged in 5 iterations with sharp error reduction. We think the reason for this good performance is that moment-based weak-form SSD implicitly carries global image information, achieving a similar effect to hierarchical registration [15] as well as being less sensitive to noise (and partial occlusion).

5.3 Elastic image deformation

In this experiment, we tested our method on a set of gray-level images undergoing elastic deformations. We synthesized deformations of MRI brain images using randomly generated second-order polynomials, i.e., the deformation basis functions were $\Gamma = (1, x, y, x^2, xy, y^2)^{\mathsf{T}}$. In addition, we added to the images salt-and-pepper noise with probability of occurrence of 0.2. Neither Domokos and Kato [1] nor Flusser et al. [4] provide implementations that address elastic shape deformation, so we compared our method with the Lucas–Kanade's method. Figure 8 shows one sequence of registration using our method. Figure 9 shows the corresponding AAE and AEP plots for our method and Lucas–Kanade's method. Under elastic deformation, the convergence time of our method doubled to about ten iterations. However, our method still converged exponentially and was much faster than the one using optical-flow.

Finally, we performed a set of experiments to estimate cell deformation. Figure 10 shows three frames from a sequence of fluorescence microscopy images of a living cell. The figure also shows a set of superimposed images depicting iterations of the registration process. We used the polynomial deformation model to represent the cell motion. Since ground-truth was not available, we show the registration quality by overlaying the source and target images. Note that, given the global nature of our polynomial deformation model, the registration quality of our method is slightly worse than methods based on local deformation models [2]. However, local deformation models require more computation. Our method can be used for approximated elastic registration, such as in real-time medical image indexing [26], where the deformation field is relatively constrained and registration accuracy is not the main concern.

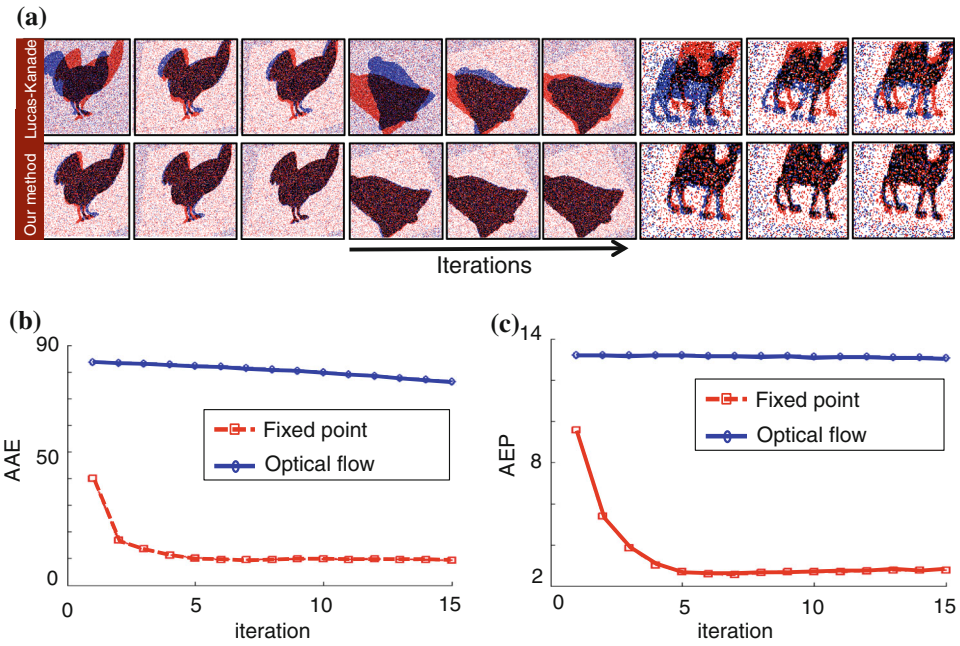

Fig. 7 **a** Registration sequence for noisy and partially occluded images. The source image (*red*) is warped to the target image (*blue*). Noise is salt-and-pepper with occurrence probability of 0.2. **b** Average angular error. **c** Average end-point error (color figure online)

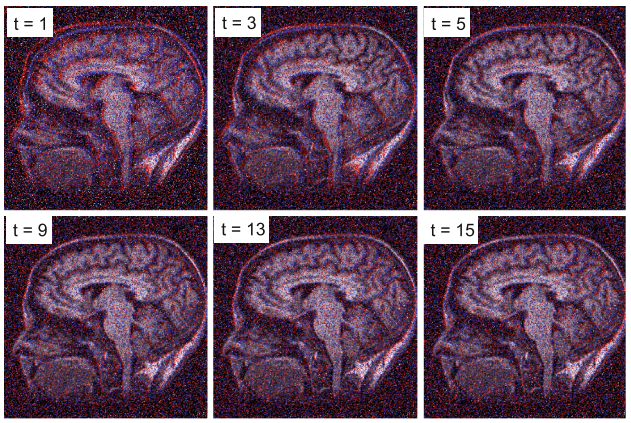

Fig. 8 Registration of brain MRI images under elastic deformation. Our method aligns the images in 15 iterations

6 Conclusion and future work

In this paper, we proposed an iterative method for image registration based on image moments. Our registration method is based on the observation that, when the deformation field between two images is modeled by polynomials, incremental changes in moments calculated on those images are related by linear equations of the deformation parameters. Our method calculates the image deformation that best matches the changes in moments of the template and target images without relying on individual pixels' intensities. Experiments showed that our method is fairly robust to noise and occlusion, and it converges in a small number of steps.

Our deformation field was limited to low-order polynomials because of numeric sensitivity of higher-order polynomials. Increased numerical stability may be obtained using orthogonal polynomials as in [4]. In addition, our method may become trapped in local minimum (see Fig. 11 for

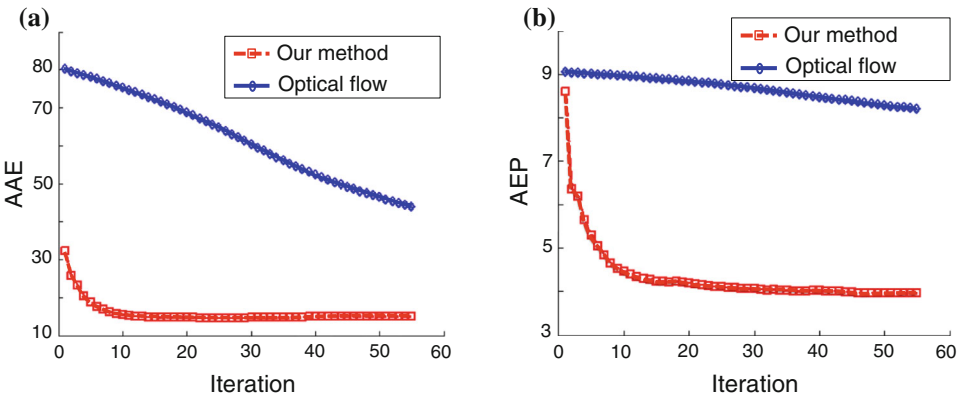

Fig. 9 Convergence of shape registration algorithms under elastic deformation. **a** Average angular error. **b** Average end-point error. Both our method and the optical-flow method converged slower for the elastic deformation case than they did for the linear deformation case. However, ours still converged faster than the optical-flow method

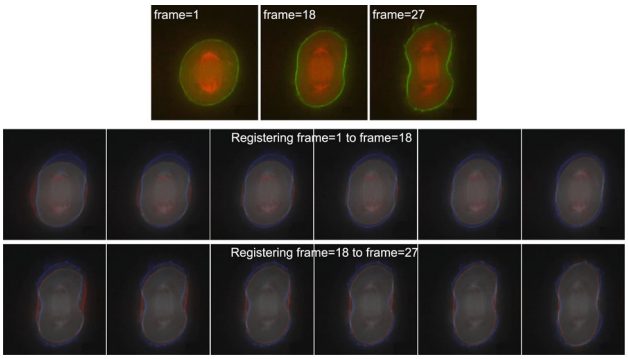

Fig. 10 Registration of deforming cells (best seen in color). *Top* Three frames of a cell undergoing elastic deformation under a fluorescent microscope. *Bottom* Inter-frame registration using our method (color figure online)

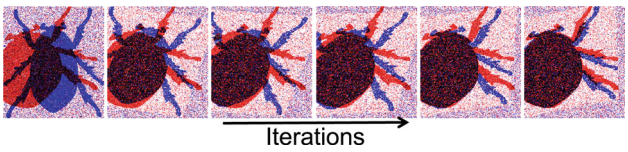

Fig. 11 Example of our method being trapped in local minima

an example). As a future work, we plan to use other integral transforms such as wavelets and Fourier transforms and study their interaction with local deformation models, such as splines [27], and meshless models [2]. We also plan to explore the application of our method in group and data-driven registration. Finally, since integral transforms are frequently used in content-adaptive compression methods [28], content-adaptive registration is also an interesting topic for future investigation.

References

1. Domokos, C., Kato, Z.: Parametric estimation of affine deformations of planar shapes. Pattern Recognit. **43**(3), 569–578 (2010)
2. Liu, W., Ribeiro, E.: A meshless method for variational nonrigid 2-D shape registration. In: International Symposium on Visual Computing (2010)
3. Ming, M.K.: Visual pattern recognition by moment invariants. Trans. Inf. Theory **IT-8**, 179–187 (1962)
4. Flusser, J., Kautsky, J., Šroubek, F.: Implicit moment invariants. Int. J. Comput. Vis. **86**(1), 72–86 (2010)
5. Liu, W., Ribeiro, E.: Estimating nonrigid shape deformation using moments. In: IEEE International Conference on Pattern Recognition (2010)
6. Zitova, B., Flusser, J.: Image registration methods: a survey. Image Vis. Comput. **21**(11), 977–1000 (2003)
7. De Castro, E., Morandi, C.: Registration of translated and rotated images using finite Fourier transforms. In: IEEE Trans. Pattern Anal. Mach. Intell. **9**(5), 700–703 (1987)
8. Chen, Q.-s., Defrise, M., Deconinck, F.: Symmetric phase-only matched filtering of fourier-mellin transforms for image registration and recognition. In: IEEE Trans. Pattern Anal. Mach. Intell. **16**, 1156–1168 (1994)
9. Lehmann, T.M.: A two-stage algorithm for model-based registration of medical images. In: IEEE International Conference on Pattern Recognition, p. 344. IEEE Computer Society (1998)
10. Sato, J., Hollinghurst, N.J.: Image registration using multi-scale texture moments. Image Vis. Comput. **13**(5), 496–513 (1995)
11. Le Moigne, J., Campbell, W.J., Cromp, R.F.: An automated parallel image registration technique based on the correlation of wavelet features. In: IEEE Trans. Geosci. Remote Sens. **40**(8), 1849–1864 (2002)
12. Zokai, S., Wolberg, G.: Image registration using log-polar mappings for recovery of large-scale similarity and projective transformations. In: IEEE Trans. Image Process. **14**(10), 1422–1434 (2005)
13. Bentoutou, Y., Taleb, N., Kpalma, K., Ronsin, J.: An automatic image registration for applications in remote sensing. In: IEEE Trans. Geosci. Remote Sens. **43**(9), 2127 (2005)
14. Shen, D., Davatzikos, C.: HAMMER: hierarchical attribute matching mechanism for elastic registration. In: IEEE Trans. Med. Imaging **21**(11), 1421–1439 (2003)
15. Lucchese, L., Doretto, G., Cortelazzo, G.M.: A frequency domain technique for range data registration. In: IEEE Trans. Pattern Anal. Mach. Intell. **24**(11), 1468–1484 (2002)
16. Ito, K., Aoki, T., Kosuge, E., Kawamata, R., Kashima, I.: Medical image registration using phase-only correlation for distorted dental radiographs. In: IEEE International Conference on Pattern Recognition, pp. 1–4 (2008)
17. Crespo, J.B.F.P., Aguiar, P.M.Q.: Revisiting complex moments for 2-D shape representation and image normalization. In: IEEE Trans. Image Process. **20**(10), 2896–2911 (2011)
18. Hoey, J., Little, J.J.: Bayesian clustering of optical flow fields. In: IEEE International Conference on Computer Vision, vol. 2, p. 1086. IEEE Computer Society (2003)
19. Flusser, J., Suk, T., Zitov, B.Inc Ebrary: *Moments and Moment Invariants in Pattern Recognition*. (Wiley, New York 2009)
20. Davies, B.: Integral Transforms and Their Applications. Springer, New York (2002)
21. Mehtre, B.M., Kankanhalli, M.S.et al. : Shape measures for content based image retrieval: a comparison. Inf. Process. Manag. **33**(3), 319–337 (1997)
22. Tian, Y., Narasimhan, S.G.: A globally optimal data-driven approach for image distortion estimation. In: IEEE International Conference on Computer Vision and Pattern Recognition (2010)
23. Rudin, W.: Real and Complex Analysis. Tata McGraw-Hill, New York (2006)
24. Lucas, B.D., Kanade, T.: An iterative image registration technique with an application to stereo vision. In: International Joint Conference on Artificial Intelligence, vol. 3, pp. 674–679 (1981)
25. Thakoor, N., Gao, J., Jung, S.: Hidden Markov model-based weighted likelihood discriminant for 2-D shape classification. In: IEEE Trans. Image Process. **16**(11), 2707–2719 (2007)
26. Liu, R., Li, S., Tan, C.L., Pang, B.C., Lim, C.C.T., Lee, C.K., Tian, Q., Zhang, Z.: Fast traumatic brain injury ct slice indexing via anatomical feature classification. In: IEEE International Conference on Image Processing, pp. 4377–4380 (2010)
27. Rueckert, D., Sonoda, L.I., Hayes, C., Hill, D.L.G., Leach, M.O., Hawkes, D.J.: Nonrigid registration using free-form deformations: application to breast MR images. In: IEEE Trans. Med. Imaging **18**(8), 712–721 (1999)
28. Chang, S.G., Yu, B., Vetterli, M.: Adaptive wavelet thresholding for image denoising and compression. In: IEEE Trans. Image Process. **9**(9), 1532–1546 (2002)